Article

Discovery Medicine 2026; 38(204): 243–255
https://doi.org/10.24976/Discov.Med.202638204.19

KDM5B Suppresses Apoptosis and Enhances Migration and Tube Formation in Skin Flaps After IR Injury via the Activation of the AMPK/KLF2 Signaling Pathway

Yuan Jiang[1], Zhao Lu[2,*]

[1]Department of Plastic Surgery, Lishui Hospital of Wenzhou Medical University (Lishui People's Hospital), 323000 Lishui, Zhejiang, China
[2]Department of Aesthetic Medicine, Lishui Hospital of Wenzhou Medical University (Lishui People's Hospital), 323000 Lishui, Zhejiang, China
*Correspondence: lz_dr688@163.com (Zhao Lu)

Submitted: 19 September 2025 Revised: 14 November 2025 Accepted: 4 December 2025 Published: 20 January 2026

Background: Skin flap ischemia/reperfusion (IR) injury contributes to reducing the survival rate in flaps after grafting. Lysine demethylase 5B (KDM5B) plays a crucial role in epigenetic regulation both during normal development and carcinogenesis. Therefore, this study aims to investigate the precise role and underlying mechanism of KDM5B in the skin flap after IR injury.
Methods: An *in vitro* skin flap model was developed in oxygen-glucose deprivation/reoxygenation (OGD/R)-treated human umbilical vein endothelial cells (HUVECs), and the expression levels of *KDM5B*, AMP-activated protein kinase (AMPK), and Kruppel-like factor 2 (KLF2) were assessed using western blot and quantitative reverse transcription polymerase chain reaction (qRT-PCR) analyses. Furthermore, cellular apoptosis rate, scratch wound healing, migration, and tube formation were assessed in treated HUVECs using flow cytometry, Transwell, and tube formation assays, respectively.
Results: KDM5B was downregulated in the skin flap after IR injury *in vivo* ($p < 0.05$). *In vitro*, *KDM5B* overexpression alleviated OGD/R-induced injury in HUVECs, as verified by the rescued cell viability ($p < 0.05$), reduced Lactate dehydrogenase (LDH) release ($p < 0.05$) and restored mitochondrial membrane potential ($p < 0.05$). Additionally, overexpression of KDM5B suppressed OGD/R-induced apoptosis ($p < 0.05$), enhanced cell migration ($p < 0.05$), and promoted tube formation ($p < 0.05$) in HUVECs. Mechanistically, *KDM5B* overexpression activated the AMPK/KLF2 signaling pathway, which was inhibited by OGD/R treatment ($p < 0.05$). The protective effects of KDM5B on apoptosis, migration, and tube formation were abolished by the AMPK inhibitor Compound C ($p < 0.05$). The *in vivo* experiments confirmed that *KDM5B* overexpression promoted skin flap survival ($p < 0.05$), reduced apoptosis ($p < 0.05$), and enhanced angiogenesis ($p < 0.05$).
Conclusion: This study is the first to demonstrate that KDM5B suppresses apoptosis and enhances migration and angiogenesis in the skin flap after IR injury through activation of the AMPK/KLF2 signaling pathway.

Keywords: Lysine demethylase 5B; skin flap ischemia/reperfusion injury; apoptosis; migration; tube-forming activities; AMPK/KLF2 signaling pathway

Introduction

Flap grafting is a primary technique used for tissue repair of defects and deformities on the body surface and is widely employed in orthopedics, microsurgery, and oral and maxillofacial procedures [1,2]. However, its application is frequently limited by ischemia-reperfusion (IR) injury, which causes oxidative stress, inflammation, and dysregulated cell proliferation, migration, and angiogenesis [3,4]. Particularly, endothelial cell apoptosis, inflammation, and excessive reactive oxygen species (ROS) production triggered by IR injury are predominant contributors to skin flap injury [5,6]. Therefore, investigating approaches that promote angiogenesis while suppressing apoptosis may improve the survival rate of skin flaps after IR injury.

Lysine demethylase 5B (KDM5B), also known as JARID1B, is a member of the KDM5 family and plays a key role in the epigenetic regulation of normal development and carcinogenesis [7]. Evidence shows that KDM5B enhances the proliferation and motility of tumor cells across several cancer types, including breast, prostate, and gastric cancers [8–10]. In the skin, it modulates mesenchymal epithelial transformation (MET) related genes and promotes epithelial cell differentiation, which is involved in barrier function [11]. Furthermore, *KDM5B* knockdown has been reported to attenuate the migration and angiogenesis in human umbilical vein endothelial cells, thereby inhibiting retinal angiogenesis in vascular disease models [12]. However, the precise role and underlying mechanisms of KDM5B in skin flaps after IR injury remain unclear.

AMP-activated protein kinase (AMPK) is a critical cellular energy sensor involved in IR injury and oxida-

tive stress [13]. Activation of AMPK improves mitochondrial function and promotes the survival of IR-induced skin flaps [6]. Moreover, KDM5B has been found to activate AMPK, thereby promoting cell proliferation and migration [8]. Given this, we hypothesized herein that KDM5B may alleviate skin flaps after IR injury by modulating the AMPK signaling pathway. In this study, oxygen-glucose deprivation/reoxygenation (OGD/R) and IR-induced skin flap models were utilized to mimic flap injury *in vitro* and *in vivo*, respectively. The study herein preliminarily explores the role of KDM5B in regulating apoptosis, migration, and tube formation in skin flaps after IR injury, suggesting its potential as a therapeutic target.

Methods and Materials

Animal Models

Male C57BL/6 mice weighing between 20 and 25 g (n = 24) were obtained from NAJINGJIANCHENG Bioengineering Institute and housed under specific-pathogen-free conditions with free access to food and water. Furthermore, mice were randomly divided into four groups (n = 6 per group): Sham, IR, IR+NC, and IR+AAV-KDM5B. Four weeks before IR surgery, 1×10^{13} viral genome particles of either adeno-associated virus 9 (AAV9) vector containing KDM5B (AAV9-KDM5B) or a control AAV9-NC (NC) were injected into mice via the tail vein. Subsequently, mice underwent IR surgery. First, the mice were anesthetized with 1% pentobarbital sodium (50 mg/kg). Afterwards, the protruding part of the sternum from the upper to the groin was selected and labeled as a 4 cm $\times$ 4 cm flap. The flap was stripped along the marked line to separate it from the underlying muscle layer. IR surgery was then performed by ligating the inferior superficial artery of the right abdominal wall and clamping the corresponding vessel on the left abdominal wall for 3 hours. IR surgery was not performed in the Sham group; instead, it received only ligation of the inferior superficial artery of the left abdominal wall as previously reported [14]. Following 72 h of reperfusion, mice were sacrificed with 150 mg/kg pentobarbital sodium and skin flaps immediately harvested.

Macroscopic Evaluation of Flap

High-resolution images of the skin flap were captured, and the viable flap area was examined using Image-Pro Plus imaging software 6.0 (Media Cybernetics, USA). The flap survival rate was calculated as follows: the survival area/total area $\times$ 100%. Tissue samples from the skin flap areas were collected for further analysis.

Cell Culture and Transfection

Human umbilical vein endothelial cells (HUVECs) were procured from the American Type Culture Collection (Cat. No. PCS-100-013 ATCC, USA) and maintained under aseptic, contamination-free conditions. The HUVECs used in this study were authenticated by short tandem repeat (STR) analysis, confirming their human origin and absence of cross-contamination, and were routinely tested for mycoplasma contamination, with all cultures confirmed to be negative prior to experiments. Cells were cultured in Dulbecco's modified Eagle's medium (DMEM; Cat. No. PM150210, Procell) containing 10% fetal bovine serum (FBS; Cat. No. A5256701, Gibco, USA) and 1% antibiotics (penicillin 100 IU/mL and streptomycin 100 µg/mL) at 37 °C with 5% CO_2.

For plasmid transfection, the full-length human *KDM5B* cDNA (**Supplementary file 1**) was cloned into the pcDNA3.1(+) vector (Cat. No. V790-20, Invitrogen, Carlsbad, CA, USA). HUVECs at 70–80% confluence were transfected with either the empty vector (negative control, NC) or the KDM5B-expressing plasmid (pcDNA3.1-KDM5B) using Lipofectamine 3000 reagent (Thermo Fisher Scientific, Waltham, MA, USA) according to the manufacturer's protocol. Transfected cells were harvested 48 hours post-transfection for subsequent experiments.

The OGD/R model was developed to mimic IR-induced skin flap injury *in vitro*. HUVECs were subjected to a 6-h hypoxic challenge in a dedicated chamber (Cat. No. 27310, Thermo Scientific, Waltham, MA, USA) infused with 95% N_2 and 5% CO_2, using glucose- and serum-free DMEM supplemented with apelin-13 and specific inhibitors. After this treatment, the medium was substituted with complete RPMI 1640 containing 10% FBS, and the cells were returned to a standard normoxic incubator for an additional 6 h of culturing (reoxygenation). Thereafter, for AMPK inhibition, cells were incubated with 8 µM Compound C (CC) (Cat. No. P5499, Sigma-Aldrich, Merck KGaA) for 30 min after OGD/R treatment.

MTT Assay

Cell viability was assessed using the MTT assay. Briefly, cells were seeded in 96-well plates at a density of 3.0×10^3 cells per well. After the indicated treatments, 20 µL of MTT solution (5 mg/mL; Sigma-Aldrich, St. Louis, MO, USA; Cat. No. M2128) was added to each well and incubated for 4 hours at 37 °C. Subsequently, the culture medium was carefully removed, and 150 µL of dimethyl sulfoxide (DMSO; Cat. No. D5879, Sigma-Aldrich, Rockville, MD, USA) was added to each well to dissolve the formed formazan crystals. The absorbance at a wavelength of 490 nm was measured using a microplate reader (Cat. No. ELx800, BioTek Instruments, Winooski, VT, USA). Cell viability was calculated using the following formula and expressed as a percentage relative to the Control group:

$$\text{Cell Viability}\,(\%) = (OD_{(sample)} - OD_{(blank)})/(OD_{(control)} - OD_{(blank)}) \times 100\%$$

LDH Release Assay

Lactate dehydrogenase (LDH) release, an indicator of cytotoxicity, was measured using a commercial LDH assay kit (Abcam, Cambridge, UK; Cat. No. ab65393) according to the manufacturer's instructions. After treatments, the cell culture supernatant was collected. The adherent cells were then lysed using the provided lysis buffer for 30 minutes at room temperature to obtain the intracellular LDH fraction. Both the supernatant and cell lysates were centrifuged at 500 ×g for 5 minutes to remove debris. Subsequently, the reaction mixture was added to the samples and incubated in the dark for 30 minutes. The absorbance was measured at 450 nm (with a reference wavelength of 650 nm) using a microplate reader (Cat. No. ELx800, BioTek Instruments). The percentage of LDH release was calculated as follows:

LDH Release (%) = [LDH activity in supernatant/LDH activity in supernatant + LDH activity in cell lysate)] × 100%.

JC-1 Staining

Mitochondrial membrane potential was assessed using the JC-1 fluorescent probe (Beyotime, Shanghai, China; Cat. No. C2005). After treatments, cells were incubated with JC-1 working solution at 37 °C for 20 minutes in the dark. Subsequently, cells were washed twice with pre-warmed JC-1 staining buffer. Fluorescence images were immediately captured using a fluorescence microscope (Cat. No. IX73, Olympus, Tokyo, Japan). JC-1 aggregates (red fluorescence, Ex/Em = 525/590 nm) indicate high $\Delta\Psi m$, while JC-1 monomers (green fluorescence, Ex/Em = 490/530 nm) indicate low $\Delta\Psi m$. For quantitative analysis, cells were also processed in a 96-well plate. After staining and washing, the fluorescence intensities of both aggregates (red) and monomers (green) were measured using a fluorescence microplate reader (Cat. No. ELx800, BioTek Instruments, Winooski, VT, USA). The ratio of red to green fluorescence intensity was calculated to represent the relative $\Delta\Psi m$.

Cell Apoptosis Assay

Cell apoptosis was quantified using an Annexin V-FITC/PI Apoptosis Detection Kit (BD Biosciences, San Jose, CA, USA; Cat. No. 556547). After treatments, cells were harvested by trypsinization (without EDTA), washed twice with cold PBS, and resuspended in 1× Binding Buffer at a concentration of 1×10^6 cells/mL. Then, 100 µL of the cell suspension was incubated with 5 µL of Annexin V-FITC and 5 µL of Propidium Iodide (PI) for 15 minutes at room temperature in the dark. Subsequently, 400 µL of 1× Binding Buffer was added to each sample. Apoptosis was analyzed within 1 hour using a BD FACSCanto II flow cytometer (BD Biosciences, Franklin Lakes, NJ, USA). Data were processed with FlowJo software (v10.8.1, BD Biosciences, Franklin Lakes, NJ, USA). Cells stained positive for Annexin V-FITC but negative for PI were considered early apoptotic, while cells positive for both Annexin V-FITC and PI were considered late apoptotic/necrotic.

Cell Migration Assay

HUVECs were seeded into 6-well plates and grown to 100% confluence. A straight scratch was created across the monolayer using a sterile 200 µL pipette tip (Cat. No. T70310333322, Thermo Fisher, USA). The cells were then gently washed with PBS to remove detached cells and incubated with fresh serum-free medium. Images of the scratch were captured at 0, 6, and 12 hours at the same location under a phase-contrast microscope (Cat. No. IX73, Olympus, Tokyo, Japan). The wound width was measured using ImageJ software (v1.54, National Institutes of Health, Bethesda, MD, USA). The relative wound width was calculated as **W_6/W_0**, or **W_12/W_0**, representing the average width at 0 h, 6 h, and 12 h.

For the Transwell assay, HUVECs were seeded into the upper chamber of an 8-µm pore size insert (Cat. No. 3422, Corning, USA), and medium containing FBS was added to the lower chamber. After 24 h of incubation, migrated cells were stained with 0.1% crystal violet (Cat. No. C6158, Sigma, USA). The number of migrated cells was quantified under a microscope (Cat. No. IX73, Olympus, Tokyo, Japan).

Tube Formation Assay

Matrigel (Cat. No. 356234, Corning, NY, USA) was thawed at 4 °C overnight. Pre-chilled 96-well plates (Cat. No.167425, Thermo Fisher Scientific) were coated with 50 µL of Matrigel per well and incubated at 37 °C for 30 minutes to allow polymerization. HUVECs, after respective treatments, were harvested and resuspended in serum-free medium. A total of 2×10^4 cells in 100 µL medium were seeded onto the polymerized Matrigel in each well. The plate was incubated at 37 °C with 5% CO_2 for 6–8 hours. Capillary-like tube structures were observed and photographed under an inverted microscope (Cat. No. IX73, Olympus, Tokyo, Japan). Tube formation was quantified by measuring the total tube length and counting the number of branching points in three randomly selected fields per well using ImageJ software (v1.54, National Institutes of Health, Bethesda, MD, USA) with the Angiogenesis Analyzer plugin.

Quantitative Real-Time PCR (qRT-PCR) Assay

Total RNA was extracted from tissues or cells using TRIzol reagent (Cat. No. 15596018, Invitrogen, Carlsbad, CA, USA). RNA concentration and purity were assessed using a NanoDrop 2000 spectrophotometer (Thermo Fisher Scientific). One microgram of total RNA was reverse transcribed into cDNA using the PrimeScript™ RT Reagent Kit with gDNA Eraser (Cat. No. RR047A, Takara, Dalian, China). qRT-PCR was performed on a QuantStudio 5 Real-Time PCR System (Applied Biosystems, Foster City,

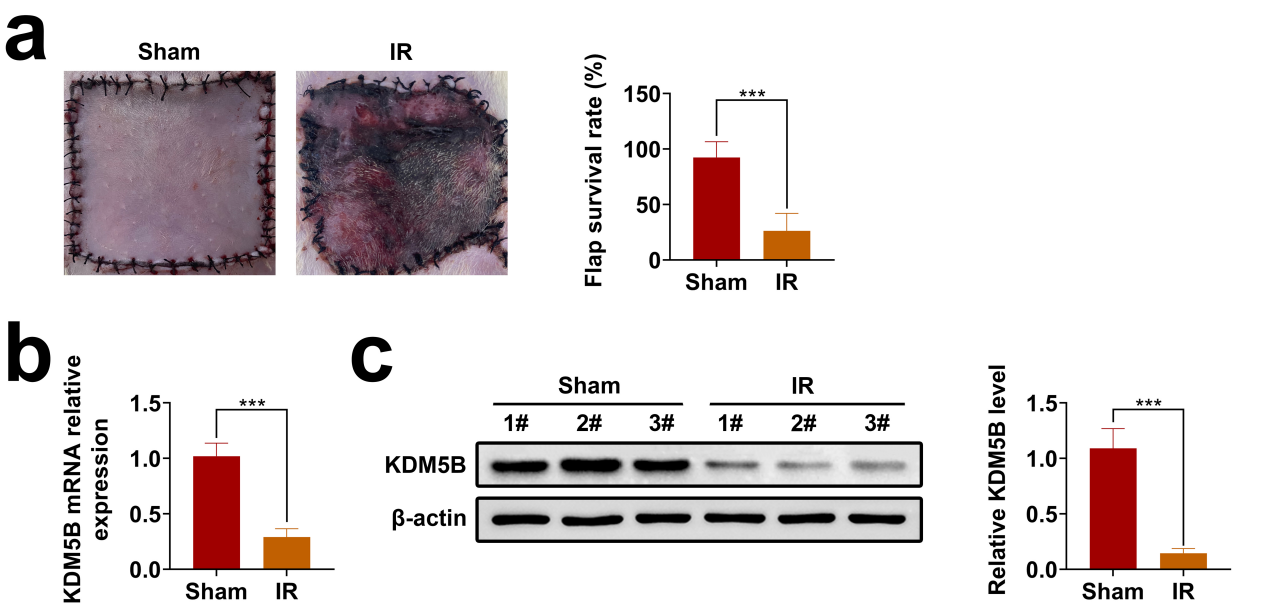

Fig. 1. Down-regulated Lysine demethylase 5B (KDM5B) in the skin flap after ischemia/reperfusion (IR) injury in mice. The mice were divided into the IR and Sham groups. Mice in the IR model group received 3-h ischemia and 72-h reperfusion (n = 6 per group). (a) Representative photographs of the abdominal skin flaps and the calculated flap survival rate. The mRNA (b) and protein (c) levels of KDM5B in skin the flap were determined using quantitative reverse transcription polymerase chain reaction (qRT-PCR) and western blotting. Each experiment was conducted in triplicate. ***$p < 0.001$.

CA, USA) using TB Green® Premix Ex Taq™ II (Cat. No. RR820A, Takara, Dalian, China). The thermocycling conditions were as follows: initial denaturation at 95 °C for 30 seconds, followed by 40 cycles of 95 °C for 5 seconds and 60 °C for 30 seconds. Each sample was run in triplicate. The relative mRNA expression levels were calculated using the $2^{-\Delta\Delta Ct}$ method, with β-actin serving as the internal control gene. Primer sequences used in qRT-PCR were as follows: mouse-β-actin-forward: 5'-GGCTATGCTCTCCCTCACG-3', mouse-β-actin-reverse: 5'-GAGCAACATAGCACAGCTTCTCTTT-3'; mouse-KDM5B-forward: 5'-ATCGCTTGCTGCACCGTTAT-3', mouse-KDM5B-reverse: 5'-CGCTCATCATCTGGCAACAG-3'.

Western Blotting

Total proteins were extracted from tissues and cells using RIPA lysis buffer (Beyotime; Cat. No. P0013B) containing protease and phosphatase inhibitors. Protein concentration was determined using a BCA Protein Assay Kit (Cat. No. P0012, Beyotime). Equal amounts of protein (30 µg per lane) were separated by 10% SDS-PAGE and transferred onto polyvinylidene difluoride (PVDF) membranes (IPVH00010, Merck Millipore, Billerica, MA, USA). After blocking with 5% non-fat milk for 1 hour at room temperature, the membranes were incubated overnight at 4 °C with the following primary antibodies: anti-KDM5B (rabbit, 1:800; Abcam, Cat. No. ab181089), anti-β-actin (mouse, 1:5000; Abcam, Cat. No. ab6276), anti-BCL2-associated X protein (BAX) (rabbit, 1:1000; Abcam, Cat. No. ab32503), anti-B-cell lymphoma 2 (BCL2) (rabbit, 1:1000; Abcam, Cat. No. ab32124), anti-Cleaved caspase-3 (rabbit, 1:1000; Abcam, Cat. No. ab32042), anti-caspase-3 (rabbit, 1:1000; Abcam, Cat. No. ab32351), anti-vascular endothelial growth factor (VEGF) (rabbit, 1:1000; Abcam, Cat. No. ab32152), anti-fibroblast growth factor 1 (FGF1) (rabbit, 1:1000; Abcam, Cat. No. ab9588), anti-PDGFA (rabbit, 1:1000; Abcam, Cat. No. ab203063), anti-p-AMPK (rabbit, 1:1000; Cell Signaling Technology, Danvers, MA, USA; Cat. No. 2535), anti-AMPK (rabbit, 1:1000; Cell Signaling Technology; Cat. No. 5831), and anti- Kruppel-like factor 2 (KLF2) (rabbit, 1:1000; Abcam; Cat. No. ab203591).

After washing, membranes were incubated with corresponding horseradish peroxidase (HRP)-conjugated secondary antibodies: goat anti-rabbit IgG (Abcam; Cat. No. ab6721) or goat anti-mouse IgG (Abcam; Cat. No. ab6789), at a dilution of 1:5000 for 1 hour at room temperature. Protein bands were visualized using an enhanced chemiluminescence (ECL) detection kit (Beyotime; Cat. No. P0018FS) and captured on a ChemiDoc™ MP Imaging System (Bio-Rad Laboratories, Hercules, CA, USA). Band intensities were quantified using Image Lab software (v6.1, Bio-Rad) and normalized to the intensity of β-actin.

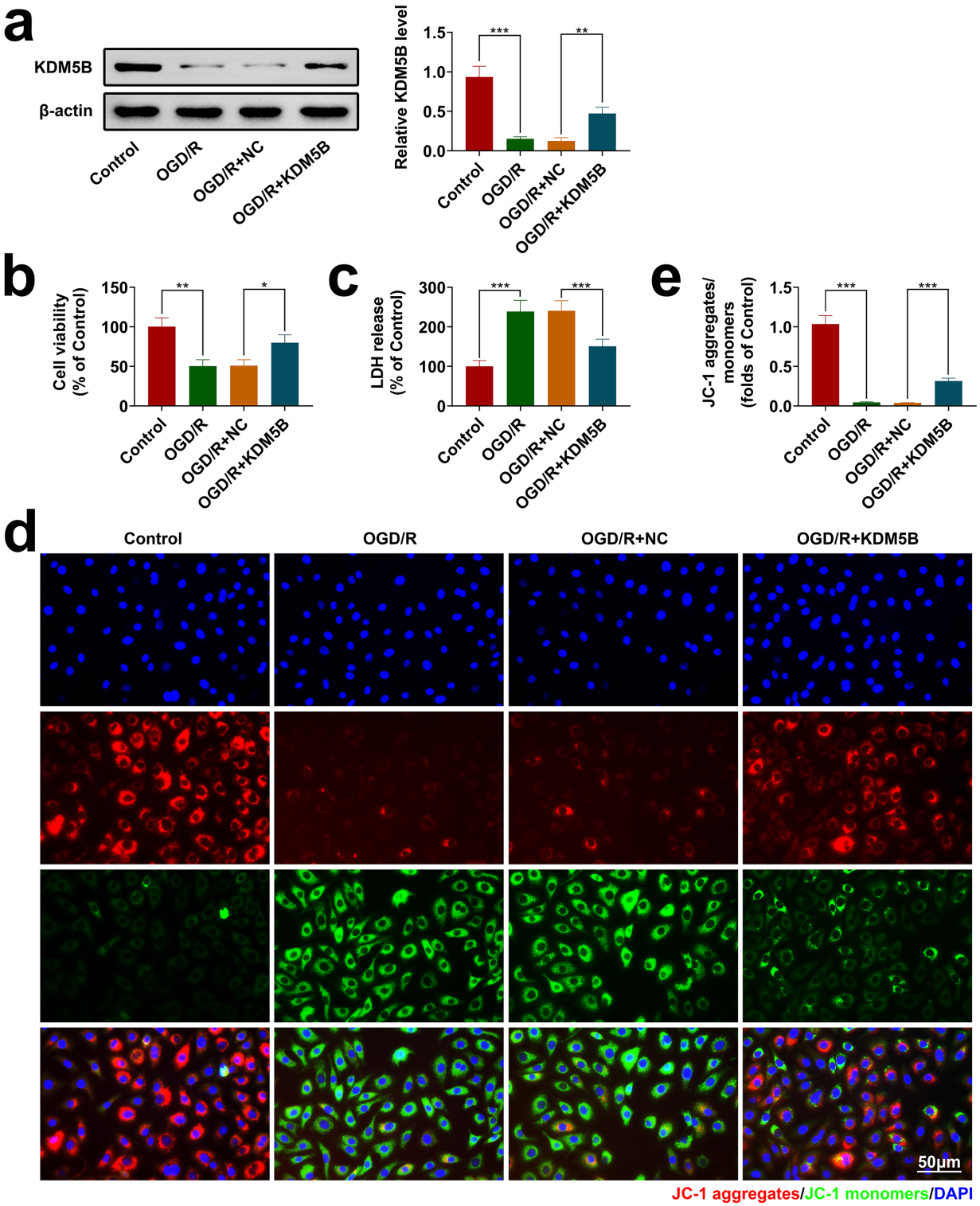

Fig. 2. KDM5B alleviates oxygen-glucose deprivation/reoxygenation (OGD/R) -induced injury in human umbilical vein endothelial cells (HUVECs). HUVECs were simulated with OGD/R to mimic the skin flap after IR injury *in vitro*. (a) KDM5B expression was assessed using Western blotting after the transfection with pcDNA.3-KDM5B. (b) HUVECs viability was determined using the MTT assay. (c) Effect of overexpressed KDM5B on OGD/R-induced Lactate dehydrogenase (LDH) release. (d,e) Quantification of immunofluorescence and fluorescence intensities of JC-1 in different groups. Each experiment was performed in triplicate. $*p < 0.05$, $**p < 0.01$, $***p < 0.001$.

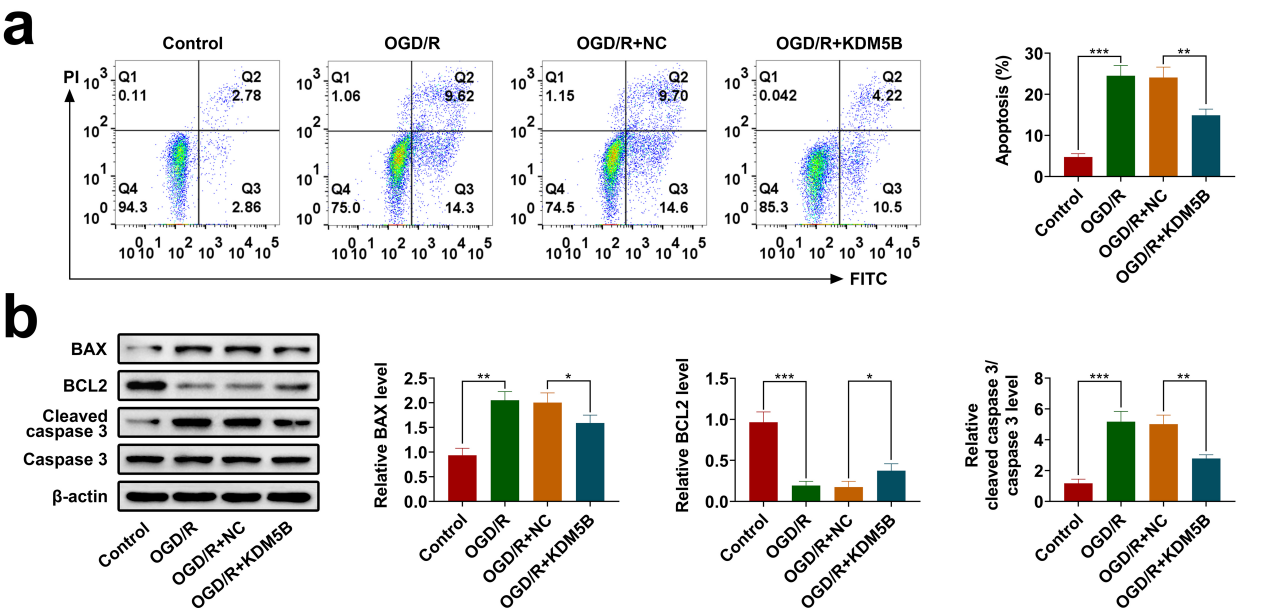

Fig. 3. KDM5B alleviates OGD/R-induced apoptosis in HUVECs. (a) Flow cytometry evaluated apoptosis in modified HUVECs. (b) The expression levels of Caspase-3, Cleaved caspase-3, B-cell lymphoma 2 (BCL2), and BCL2-associated X protein (BAX) in modified HUVECs were assessed using WB analysis. Each experiment was repeated three times. *$p < 0.05$, **$p < 0.01$, ***$p < 0.001$.

Immunohistochemistry

Mouse skin samples were fixed using 4% paraformaldehyde. Following dehydration, they were embedded in paraffin and sectioned at a thickness of 4 µm. For immunofluorescence, all slices were first deparaffinized with xylene. After rehydration, antigen retrieval was conducted in sodium citrate buffer. Once the sections reached room temperature, they were incubated in a blocking solution composed of 3% BSA (Beyotime, Cat. No. ST025), 0.2% Triton X-100 (Aladdin, Cat. No.T109027) in PBS (Procell, PB180327). Following standard deparaffinization, tissue sections were incubated with a primary antibody targeting CD31 (Abcam, ab222783; 1/100) overnight at 4 °C. After washing, Goat Anti-Rabbit IgG H&L (Alexa Fluor® 488) (Abcam, ab150077, 1/5000) was applied for 2 hours at room temperature. Nuclei were subsequently counterstained with DAPI (Beyotime, Cat. No. C1002) for 10 minutes. Finally, the samples were mounted and visualized using a fluorescence microscope (Cat. No. IX73, Olympus, Tokyo, Japan). The microvessel density (MVD) was calculated by the branch points of the formed tubes scanned and quantified in five fields.

To detect cell apoptosis in skin sections, a TUNEL assay was performed using a commercial kit (Promega, G3250) following the provided protocol. After the staining procedure, sections were counterstained with DAPI. Images were captured using an inverted fluorescence microscope (Cat. No. IX73, Olympus, Tokyo, Japan).

Statistical Analysis

All data are presented as mean ± standard deviation (SD) from at least three independent experiments. Statistical analysis was performed using SPSS 22.0 software (IBM Corp., Armonk, NY, USA). The Shapiro-Wilk test was used to assess normality, and Levene's test was used to assess homogeneity of variances. For comparisons between two groups, an unpaired two-tailed Student's *t*-test was used. For comparisons among more than two groups, one-way analysis of variance (ANOVA) was performed, followed by Tukey's post-hoc test for multiple comparisons. A *p*-value of less than 0.05 was considered statistically significant.

Results

Down-Regulation of KDM5B in the Skin Flap After IR Injury in Mice

The 3-h ischemia and 72-h reperfusion IR model was developed to assess the role of KDM5B in the skin flap after IR injury. In the Sham group, skin flaps appeared pink and elastic, while the IR group showed brown, inelastic skin with a significant reduction in flap survival rate ($p < 0.05$, Fig. 1a). Additionally, both *KDM5B* mRNA and protein levels were substantially decreased in the skin flaps of IR mice ($p < 0.05$, Fig. 1b,c). These findings indicate that KDM5B is downregulated in the skin flap following IR injury in mice.

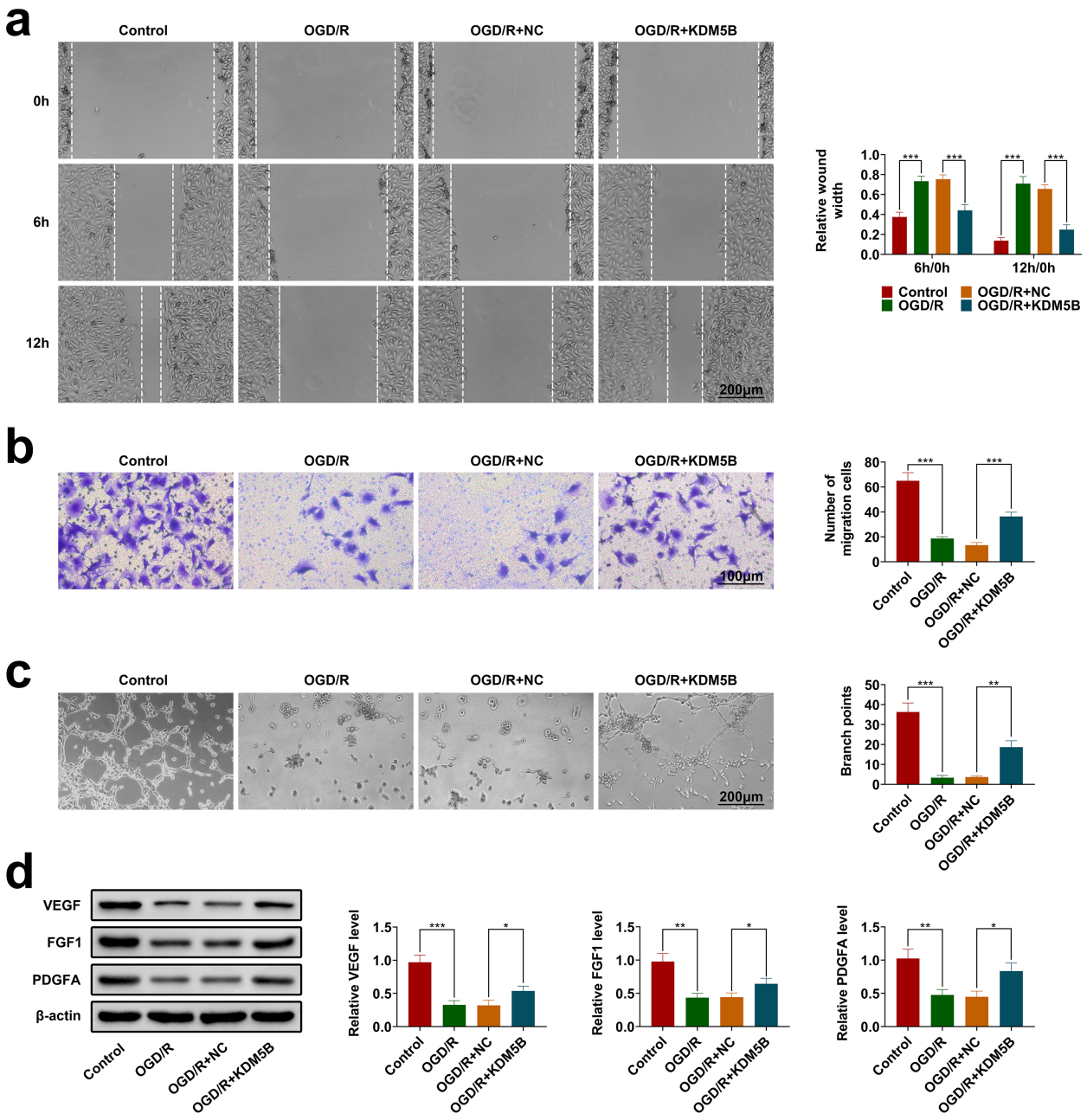

Fig. 4. KDM5B enhances migration and tube formation capabilities in HUVECs. (a) Phase contrast microscopic images of HUVECs at 0, 6, and 12 h after the scratch wound healing assay. (b) Images of migrated HUVECs were evaluated using the Transwell assay. (c) Images of tube-forming HUVECs were captured after the tube formation assay. (d) The expression levels of vascular endothelial growth factor (VEGF), fibroblast growth factor 1 (FGF1), and platelet-derived growth factor α polypeptide (PDGFA) were assessed using Western blot analysis. Each experiment was repeated three times. *$p < 0.05$, **$p < 0.01$, ***$p < 0.001$.

KDM5B Attenuates OGD/R-Induced Injury in HUVECs

The *in vitro* OGD/R model was developed in HUVECs to explore the role of KDM5B in IR-induced skin flap injury. Initially, KDM5B was successfully overexpressed in OGD/R-treated HUVECs. (Fig. 2a). *KDM5B* overexpression substantially attenuated the OGD/R-induced decline in cell viability ($p < 0.05$, Fig. 2b). Moreover, OGD/R treatment significantly elevated LDH release, which was suppressed by high KDM5B expression ($p < 0.05$, Fig. 2c). Furthermore, mitochondrial membrane potential was reduced after OGD/R stimulation, and this reduction was partially restored by overexpressed KDM5B ($p < 0.05$, Fig. 2d,e). Overall, these results demonstrate that KDM5B alleviates OGD/R-induced injury in HUVECs and exerts a protective effect.

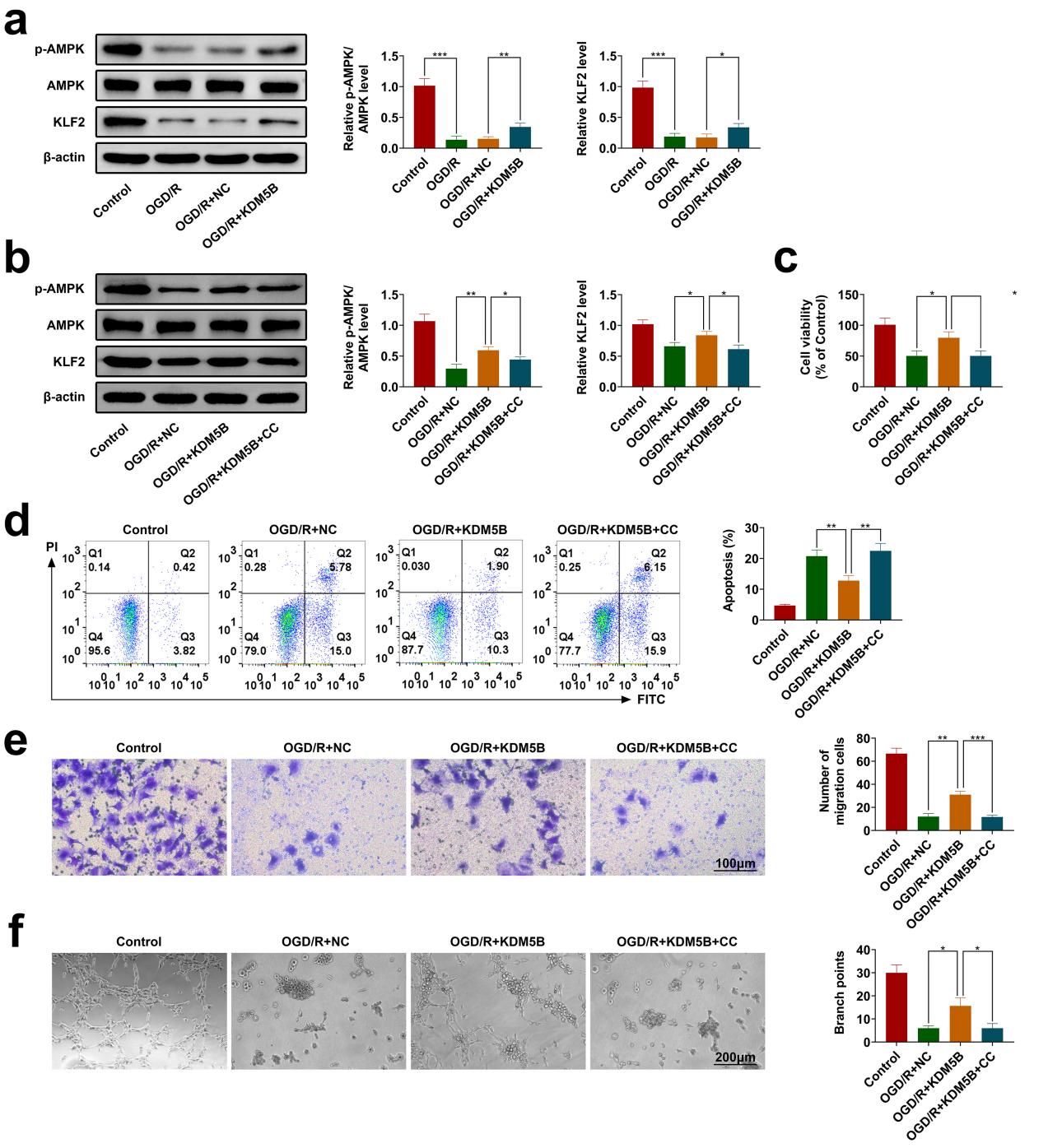

Fig. 5. KDM5B alleviates OGD/R-induced apoptosis and enhances migration and tube formation in HUVECs by activating the AMPK/KLF2 signaling pathway. (a) Western blotting showed that *KDM5B* overexpression increased the levels of p-AMPK and KLF2, which were downregulated after OGD/R treatment. (b) The AMPK inhibitor Compound C (CC) inhibited KDM5B-induced upregulation of p-AMPK and KLF2, confirming pathway deactivation. (c) KDM5B's protective effect on cell viability (measured by MTT assay) was abolished after CC treatment. (d) KDM5B anti-apoptotic effect (measured by flow cytometry) was reversed after CC treatment. (e) KDM5B pro-migratory effect (assessed by Transwell assay) was inhibited following CC treatment. (f) KDM5B-induced tube formation was attenuated after CC treatment. Each experiment was performed in triplicate. $*p < 0.05$, $**p < 0.01$, $***p < 0.001$. AMPK, AMP-activated protein kinase; KLF2, Kruppel-like factor 2.

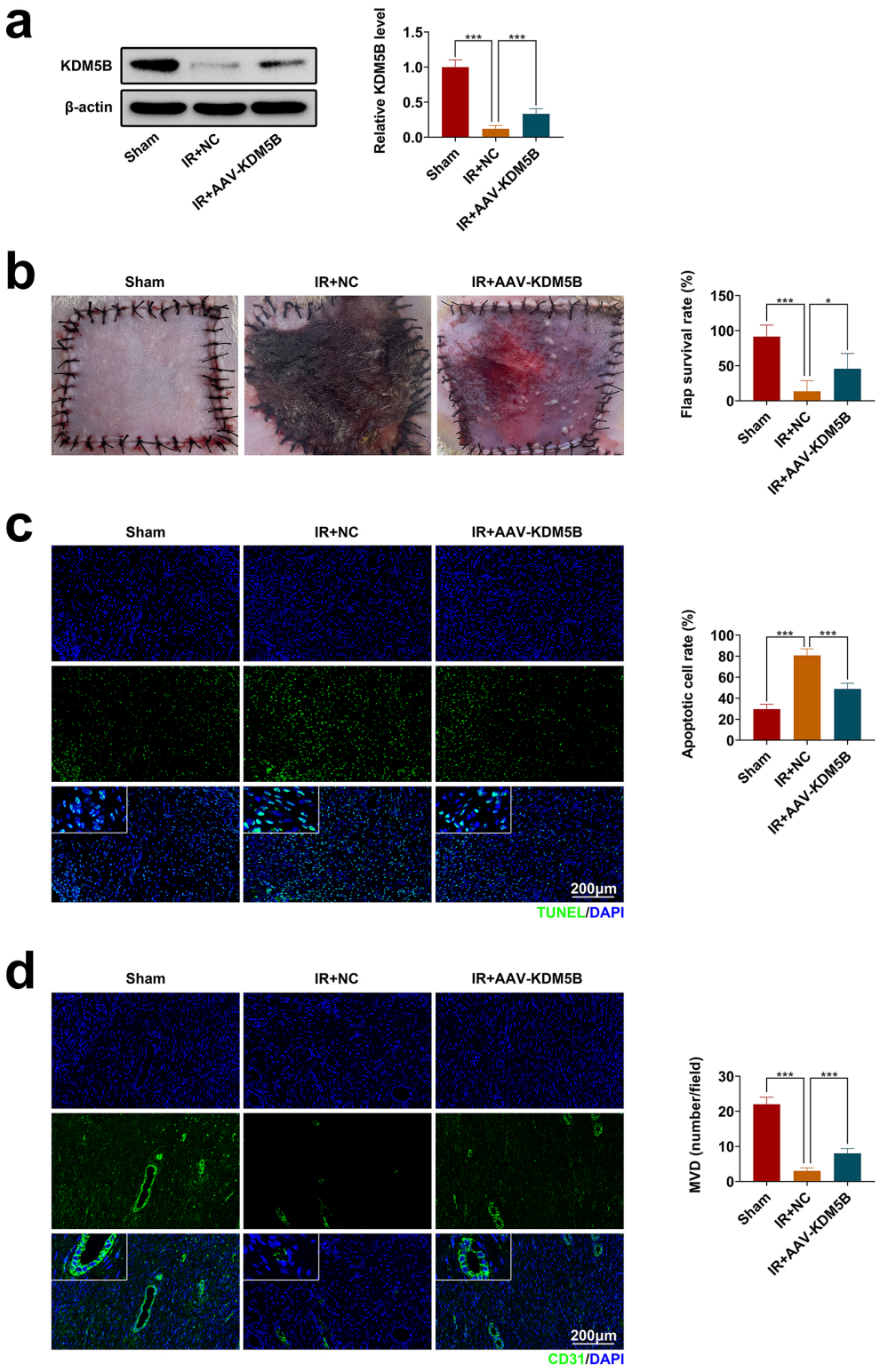

Fig. 6. KDM5B promotes skin flap survival *in vivo*. Mice were administered AAV-KDM5B before IR treatment (n = 6 per group). (a) KDM5B expression was assessed using Western blotting. (b) The flap survival rate was calculated. (c) Apoptosis was evaluated using the TUNEL staining assay. (d) Tube-forming activities were determined by CD31 immunofluorescence. Each experiment was conducted in triplicate. *$p < 0.05$, ***$p < 0.001$.

KDM5B Alleviates OGD/R-Induced Apoptosis in HUVECs

A decrease in mitochondrial membrane potential, indicative of an increase in mitochondrial depolarization, is a hallmark of apoptosis [15]. As compared to the Control group, OGD/R-simulated HUVECs showed a higher apoptotic rate, which was inhibited by *KDM5B* overexpression ($p < 0.05$, Fig. 3a). However, OGD/R treatment increased the expression of pro-apoptotic protein BAX and cleaved caspase-3 while decreasing anti-apoptotic protein BCL2, and these changes were reversed after *KDM5B* overexpression ($p < 0.05$, Fig. 3b). These results reveal that KDM5B alleviates OGD/R-induced apoptosis in HUVECs.

Evidence indicates that severe ischemia can impair arterial inflow and inhibit venous outflow within the flap, eventually leading to tissue necrosis [16]. Scratch wound healing and Transwell migration assays were performed to determine the role of KDM5B in HUVEC migration under OGD/R conditions. OGD/R treatment delayed scratch wound closure, whereas *KDM5B* overexpression substantially promoted wound closure in HUVECs ($p < 0.05$, Fig. 4a). Similarly, OGD/R treatment reduced the number of migrated HUVECs, and this reduction was attenuated by *KDM5B* overexpression ($p < 0.05$, Fig. 4b).

Furthermore, OGD/R treatment reduced the formation of new capillary-like tube meshes, whereas *KDM5B* overexpression promoted tube formation ($p < 0.05$, Fig. 4c). Western blot analysis further revealed that OGD/R treatment significantly decreased the expression of VEGF, FGF1 and PDGFA, while *KDM5B* overexpression restored and increased their levels ($p < 0.05$, Fig. 4d). These findings demonstrate that KDM5B enhances both migratory and tube-forming capabilities in HUVECs.

KDM5B Enhances Migration and Tube Formation in HUVECs

KDM5B suppressed OGD/R-induced apoptosis and enhanced migration and tube-forming activities in HUVECs via activating AMPK/KLF2 signaling pathway. As a key downstream effector of AMPK signaling, the transcription factor KLF2 is pivotal in promoting endothelial cell migration and angiogenesis. Therefore, to investigate whether KDM5B exerts its function through the AMPK/KLF2 pathway, we evaluated the expression of phosphorylated AMPK and KLF2. Interestingly, the results showed that OGD/R treatment decreased phosphorylation of AMPK and KLF2 expression, which were partly rescued by overexpression of KDM5B ($p < 0.05$, Fig. 5a). To identify the relationship between of KDM5B and AMPK/KLF2 signaling pathway, the Compound C (CC), an AMPK inhibitor, was performed. As illustrated in Fig. 5b, CC could efficiently deactivate AMPK/KLF2 signaling pathway via suppressing phosphorylation of AMPK and KLF2 expression ($p < 0.05$, Fig. 5b). As predicted, KDM5B overexpression promoted cell viability and inhibited apoptosis in HUVECs, and these protective effects were reversed by CC treatment ($p < 0.05$, Fig. 5c,d). More importantly, overexpression of KDM5B enhanced migration and tube-forming activities in HUVECs, which were reduced by CC treatment (textitp < 0.05, Fig. 5e,f). Our findings concluded that KDM5B suppressed OGD/R-induced apoptosis and enhanced migration and tube-forming activities in HUVECs via activating AMPK/KLF2 signaling pathway.

KDM5B Promotes Skin Flap Survival In Vivo

AAV-KDM5B administration substantially increased KDM5B expression in mice ($p < 0.05$, Fig. 6a). The IR+AAV-KDM5B group showed a higher flap survival than the IR+NC group ($p < 0.05$, Fig. 6b). TUNEL assay confirmed that IR-induced cell apoptosis, which was ameliorated by *KDM5B* overexpression ($p < 0.05$, Fig. 6c). Furthermore, IR treatment decreased CD31 expression, and *KDM5B* overexpression restored CD31 levels, indicating that AAV-KDM5B rescued the IR-induced suppression of tube-forming capability ($p < 0.05$, Fig. 6d). These results imply that KDM5B promotes skin flap survival *in vivo*.

Discussion

KDM5B is an evolutionarily conserved member of the KDM5 family, serving as a transcriptional repressor [17]. In this study, KDM5B was downregulated in skin flaps after IR injury. The *in vitro* skin flap model was developed using OGD/R-treated HUVECs, in which *KDM5B* overexpression alleviated OGD/R-induced injury. In gain-of-function experiments, *KDM5B* overexpression suppressed cell apoptosis, and enhanced both migratory and tube-forming capabilities in OGD/R-treated HUVECs. Mechanistically, inhibition of the AMPK/KLF2 signaling pathway abolished the protective effects of KDM5B on OGD/R-induced apoptosis, as well as on migration and tube formation in these cells. Consistent with these observations, *in vivo* overexpression of KDM5B promoted skin flap survival following IR injury.

These findings reveal that KDM5B suppresses apoptosis and enhances migration and tube formation in the skin flaps after IR injury by activating the AMPK/KLF2 signaling pathway. This provides a promising therapy approach to enhance skin flap survival. To our knowledge, this is the first evidence supporting the protective role of KDM5B in skin flap IR injury, providing novel mechanistic insights and identifying a translationally crucial therapeutic target.

Growing evidence indicates that apoptosis occurs in clinical tissues and in flap IR injury animal models [18]. Apoptosis plays a vital role in skin flap IR injury, likely through the regulation of apoptosis-related proteins [19, 20]. BAX and BCL2 can form heteropolymers that enhance mitochondrial membrane permeability and increase cytochrome C release, thereby inducing the caspase cascades and resulting in cell death [21]. In contrast, BAX promotes cytochrome C release and apoptosis, while BCL2

inhibits the caspase-dependent apoptotic pathway and suppresses cytochrome C release, thereby inhibiting overall apoptosis [22,23]. Previous studies have demonstrated that IR-induced skin flap is linked to upregulation of cleaved caspase-3 and BAX, and downregulation of BCL2 *in vivo* [18,24]. Furthermore, IR treatment in our study increased cleaved caspase-3 and BAX levels and decreased BCL2 expression. Although KDM5B has been reported as cancerogenic, promoting cancer cell proliferation in various cancer types, including gastric, hepatocellular, breast, and glioma [25]. Our findings demonstrate that KDM5B upregulation reversed these IR-induced alterations in apoptosis-related proteins, supporting an anti-apoptotic role in IR-injured skin flaps. However, the molecular mechanisms underlying this effect remain to be fully elucidated.

The suppression of tube formation is associated with cell death in the skin flap after IR injury. Flap necrosis occurs when blood flow to the distal portion becomes insufficient, whereas early initiation of angiogenesis can improve flap survival [26]. Restoration of blood supply depends on the initiation, elongation, and recanalization of vessels from the pedicle to the distal region. Activation of the apelin/angiotensin II protein J (APJ) axis has been reported to enhance vascular migration and angiogenesis under relative hypoxic conditions in skin flaps [6]. Previous research revealed that KDM5B knockout attenuated angiogenesis and metastasis [12]. Similarly, our findings demonstrated that KDM5B enhances migration and tube formation *in vitro*. Based on these results, we hypothesized that *KDM5B* overexpression enhances vascular migration and angiogenesis, thereby restoring blood flow and supporting skin flap survival after IR injury. However, the specific mechanisms by which KDM5B modulates cell migration and angiogenesis remain completely unexplored.

Previous studies have shown that *KDM5B* knockdown suppresses breast cancer cell proliferation and migration via AMPK deactivation [8]. Additionally, AMPK activation has been recognized to promote skin flap survival [27]. Considering that KLF2 overexpression upregulates VEGF expression and enhances migration and tube formation, the AMPK-KLF2 signaling pathway mediated the pro-angiogenic effects in endothelial cells [28,29]. In this study, we observed that OGD/R treatment suppressed the AMPK/KLF2 signaling pathway, whereas *KDM5B* overexpression reversed this inhibitory effect. AMPK, a physiological energy sensor, is activated under hypoxic stress through increased intracellular AMP levels, thereby enhancing endothelial cell survival and stimulating angiogenesis [30]. The anti-apoptotic, pro-migration and pro-angiogenic effects of KDM5B were suppressed by AMPK inhibition, indicating that KDM5B exerts its protective functions by activating the AMPK/KLF2 signaling axis.

This study has several limitations which should be considered before interpreting these results. First, additional clinical assessments were required to further support these observations. Second, it remains to be determined whether KDM5B exerts therapeutic effects through mechanisms independent of the AMPK/KLF2 pathway. Lastly, other therapeutic targets of apelin have not yet been identified, which may hold additional therapeutic potential and warrant further investigations.

Conclusion

The present study reveals that *KDM5B* overexpression enhances skin flap survival after IR injury by promoting angiogenesis and inhibiting apoptosis both *in vivo* and *in vitro*, and these impacts are likely mediated by activation of the AMPK/KLF2 signaling pathway.

Availability of Data and Materials

All data generated or analyzed during this study are included in this published article.

Author Contributions

YJ and ZL contributed to the study conception and design. Material preparation and the experiments were performed by YJ. Data collection and analysis were performed by YJ and ZL. The first draft of the manuscript was written by ZL, and both authors contributed to the critical revision of the manuscript for important intellectual content. Both authors read and approved the final manuscript and agreed to be accountable for all aspects of the work.

Ethics Approval and Consent to Participate

Animal experiments were conducted following the Guidelines for the Care and Use of Laboratory Animals, and the study protocols were approved by the Ethics Committee of Lishui Hospital of Wenzhou Medical University (Approval No. KYXX-2024472). All animal experiments were conducted in compliance with the ARRIVE guidelines and in accordance with the U.K. Animals (Scientific Procedures) Act 1986 and associated guidelines, EU Directive 2010/63/EU for animal experiments.

Acknowledgment

Not applicable.

Funding

This research received no external funding.

Conflict of Interest

The authors declare no conflict of interest.

Supplementary Material

Supplementary material associated with this article can be found, in the online version, at https://doi.org/10.24976/Discov.Med.202638204.19.

References

[1] Inagaki T, Morino T, Takagi R, Yamato M, Koizuka I, Yaguchi Y. Transplantation of autologous oral mucosal epithelial cell sheets inhibits the development of acquired external auditory canal atresia in a rabbit model. Acta Biomaterialia. 2020; 110: 141–152. https://doi.org/10.1016/j.actbio.2020.04.031.

[2] Varghese BT, Vijayakumar P, Ani Raj R, Thomas S. Salvaging skin loss of free fibular osteo-cutaneous flaps in oral oncological reconstruction. Oral Oncology. 2019; 97: 131–132. https://doi.org/10.1016/j.oraloncology.2019.08.021.

[3] Winkles JA. The TWEAK-Fn14 cytokine-receptor axis: Discovery, biology and therapeutic targeting. Nature Reviews. Drug Discovery. 2008; 7: 411–425. https://doi.org/10.1038/nrd2488.

[4] Pu CM, Liu CW, Liang CJ, Yen YH, Chen SH, Jiang-Shieh YF, *et al*. Adipose-Derived Stem Cells Protect Skin Flaps against Ischemia/Reperfusion Injury via IL-6 Expression. The Journal of Investigative Dermatology. 2017; 137: 1353–1362. https://doi.org/10.1016/j.jid.2016.12.030.

[5] Bai Y, Han YD, Yan XL, Ren J, Zeng Q, Li XD, *et al*. Adipose mesenchymal stem cell-derived exosomes stimulated by hydrogen peroxide enhanced skin flap recovery in ischemia-reperfusion injury. Biochemical and Biophysical Research Communications. 2018; 500: 310–317. https://doi.org/10.1016/j.bbrc.2018.04.065.

[6] Lou ZL, Zhang CX, Li JF, Chen RH, Wu WJ, Hu XF, *et al*. Apelin/APJ-Manipulated CaMKK/AMPK/GSK3β Signaling Works as an Endogenous Counterinjury Mechanism in Promoting the Vitality of Random-Pattern Skin Flaps. Oxidative Medicine and Cellular Longevity. 2021; 2021: 8836058. https://doi.org/10.1155/2021/8836058.

[7] Xhabija B, Kidder BL. KDM5B is a master regulator of the H3K4-methylome in stem cells, development and cancer. Seminars in Cancer Biology. 2019; 57: 79–85. https://doi.org/10.1016/j.semcancer.2018.11.001.

[8] Zhang ZG, Zhang HS, Sun HL, Liu HY, Liu MY, Zhou Z. KDM5B promotes breast cancer cell proliferation and migration via AMPK-mediated lipid metabolism reprogramming. Experimental Cell Research. 2019; 379: 182–190. https://doi.org/10.1016/j.yexcr.2019.04.006.

[9] Li G, Kanagasabai T, Lu W, Zou MR, Zhang SM, Celada SI, *et al*. KDM5B Is Essential for the Hyperactivation of PI3K/AKT Signaling in Prostate Tumorigenesis. Cancer Research. 2020; 80: 4633–4643. https://doi.org/10.1158/0008-5472.CAN-20-0505.

[10] Wang Z, Tang F, Qi G, Yuan S, Zhang G, Tang B, *et al*. KDM5B is overexpressed in gastric cancer and is required for gastric cancer cell proliferation and metastasis. American Journal of Cancer Research. 2014; 5: 87–100.

[11] Sun X, Li Z, Niu Y, Zhao L, Huang Y, Li Q, *et al*. Jarid1b promotes epidermal differentiation by mediating the repression of Ship1 and activation of the AKT/Ovol1 pathway. Cell Proliferation. 2019; 52: e12638. https://doi.org/10.1111/cpr.12638.

[12] Fork C, Gu L, Hitzel J, Josipovic I, Hu J, SzeKa Wong M, *et al*. Epigenetic Regulation of Angiogenesis by JARID1B-Induced Repression of HOXA5. Arteriosclerosis, Thrombosis, and Vascular Biology. 2015; 35: 1645–1652. https://doi.org/10.1161/ATVBAHA.115.305561.

[13] Yang N, Yu G, Lai Y, Zhao J, Chen Z, Chen L, *et al*. A snake cathelicidin enhances transcription factor EB-mediated autophagy and alleviates ROS-induced pyroptosis after ischaemia-reperfusion injury of island skin flaps. British Journal of Pharmacology. 2024; 181: 1068–1090. https://doi.org/10.1111/bph.16268.

[14] Wang Y, Wu Y, Zhou M, Wang P, Luo J, Rui Y. GRK2 deletion improves the function of skin flap following ischemia-reperfusion injury by regulating Drp1. American Journal of Translational Research. 2021; 13: 223–233.

[15] Liu L, Huang S, Xu M, Gong Y, Li D, Wan C, *et al*. Isoquercitrin protects HUVECs against high glucose induced apoptosis through regulating p53 proteasomal degradation. International Journal of Molecular Medicine. 2021; 48: 122. https://doi.org/10.3892/ijmm.2021.4955.

[16] Li J, Chen H, Lou J, Bao G, Wu C, Lou Z, *et al*. Exenatide improves random-pattern skin flap survival via TFE3 mediated autophagy augment. Journal of Cellular Physiology. 2021; 236: 3641–3659. https://doi.org/10.1002/jcp.30102.

[17] Harrington J, Wheway G, Willaime-Morawek S, Gibson J, Walters ZS. Pathogenic KDM5B variants in the context of developmental disorders. Biochimica et Biophysica Acta. Gene Regulatory Mechanisms. 2022; 1865: 194848. https://doi.org/10.1016/j.bbagrm.2022.194848.

[18] Liu B, Xu Q, Wang J, Lin J, Pei Y, Cui Y, *et al*. Recombinant human growth hormone treatment of mice suppresses inflammation and apoptosis caused by skin flap ischemia-reperfusion injury. Journal of Cellular Biochemistry. 2019; 120: 18162–18171. https://doi.org/10.1002/jcb.29122.

[19] Kellermeyer R, Heydman LM, Mastick GS, Kidd T. The Role of Apoptotic Signaling in Axon Guidance. Journal of Developmental Biology. 2018; 6: 24. https://doi.org/10.3390/jdb6040024.

[20] Qian W, Wang Z, Xu T, Li D. Anti-apoptotic effects and mechanisms of salvianolic acid A on cardiomyocytes in ischemia-reperfusion injury. Histology and Histopathology. 2019; 34: 223–231. https://doi.org/10.14670/HH-18-048.

[21] Zhang Y, Yang X, Ge X, Zhang F. Puerarin attenuates neurological deficits via Bcl-2/Bax/cleaved caspase-3 and Sirt3/SOD2 apoptotic pathways in subarachnoid hemorrhage mice. Biomedicine & Pharmacotherapy = Biomedecine & Pharmacotherapie. 2019; 109: 726–733. https://doi.org/10.1016/j.biopha.2018.10.161.

[22] Yamaguchi R, Lartigue L, Perkins G. Targeting Mcl-1 and other Bcl-2 family member proteins in cancer therapy. Pharmacology & Therapeutics. 2019; 195: 13–20. https://doi.org/10.1016/j.pharmthera.2018.10.009.

[23] Ugarte-Uribe B, García-Sáez AJ. Apoptotic foci at mitochondria: in and around Bax pores. Philosophical Transactions of the Royal Society of London. Series B, Biological Sciences. 2017; 372: 20160217. https://doi.org/10.1098/rstb.2016.0217.

[24] Xin D, Quan R, Zeng L, Xu C, Tang Y. Lipoxin A4 protects rat skin flaps against ischemia-reperfusion injury through inhibiting cell apoptosis and inflammatory response induced by endoplasmic reticulum stress. Annals of Translational Medicine. 2020; 8: 1086. https://doi.org/10.21037/atm-20-5549.

[25] Guo JC, Liu Z, Yang YJ, Guo M, Zhang JQ, Zheng JF. KDM5B promotes self-renewal of hepatocellular carcinoma cells through the microRNA-448-mediated YTHDF3/ITGA6 axis. Journal of Cellular and Molecular Medicine. 2021; 25: 5949–5962. https://doi.org/10.1111/jcmm.16342.

[26] Moon JH, Rhee YH, Ahn JC, Kim B, Lee SJ, Chung PS. Enhanced survival of ischemic skin flap by combined treatment with bone marrow-derived stem cells and low-level light irradiation. Lasers in Medical Science. 2018; 33: 1–9. https://doi.org/10.1007/s10103-017-2312-9.

[27] Wu H, Ding J, Li S, Lin J, Jiang R, Lin C, *et al*. Metformin Promotes the Survival of Random-Pattern Skin Flaps by Inducing

Autophagy via the AMPK-mTOR-TFEB signaling pathway. International Journal of Biological Sciences. 2019; 15: 325–340. https://doi.org/10.7150/ijbs.29009.

[28] Wang D, Song Y, Zhang J, Pang W, Wang X, Zhu Y, *et al*. AMPK-KLF2 signaling pathway mediates the proangiogenic effect of erythropoietin in endothelial colony-forming cells. American Journal of Physiology. Cell Physiology. 2017; 313: C674–C685. https://doi.org/10.1152/ajpcell.00257.2016.

[29] Chen GH, Li XL, Deng YQ, Zhou FM, Zou WQ, Jiang WX, *et al*. The Molecular Mechanism of EPO Regulates the Angiogenesis after Cerebral Ischemia through AMPK-KLF2 Signaling Pathway. Critical Reviews in Eukaryotic Gene Expression. 2019; 29: 105–112. https://doi.org/10.1615/CritRevEukaryotGeneExpr.2019029018.

[30] Zhao Y, Ye S, Lin J, Liang F, Chen J, Hu J, *et al*. NmFGF1-Regulated Glucolipid Metabolism and Angiogenesis Improves Functional Recovery in a Mouse Model of Diabetic Stroke and Acts *via* the AMPK Signaling Pathway. Frontiers in Pharmacology. 2021; 12: 680351. https://doi.org/10.3389/fphar.2021.680351.